Apoptosis (2012) 17:132–142
DOI 10.1007/s10495-011-0668-z

ORIGINAL PAPER

Activation of apoptotic signalling events in human embryonic stem cells upon Coxsackievirus B3 infection

Leonardo Romorini · María E. Scassa · Guillermo Videla Richardson · Carolina Blüguermann · Carolina Jaquenod de Giusti · María Questa · Damián D. Fernandez Espinosa · Ricardo M. Gómez · Gustavo E. Sevlever · Santiago G. Miriuka

Published online: 20 October 2011

Abstract Human embryonic stem cells (hESCs) are self-renewing pluripotent cells that can differentiate to a wide range of specialized cells and hold great promise as models for human development and disease, as well as for drug discovery and cell-replacement therapies. Group B Coxsackie viruses (CVBs) produce acute myocarditis, pancreatitis, non-septic meningitis and encephalitis in neonates, children and young adults. Moreover, CVBs can produce spontaneous miscarriage after early embryo infection. It was reported that hESCs express CVBs receptors and are susceptible to CVB3 infection. Apoptosis is one of the hallmarks of CVBs infection although details regarding CVB3 involvement in the apoptotic processes remain elusive. In order to evaluate the mechanisms of cell death induced by CVB3 in these pluripotent cells, we infected HUES-5 (H5) and WA01 (H1) hESC lines with CVB3. After validating the maintenance of stemness in these hESC lines when grown as confluent monolayers in feeder-free conditions, we analysed several aspects of programmed cell death triggered by CVB3. In all cases, we detected chromatin condensation, DNA fragmentation and caspase-9 and 3 cleavages. Moreover, we observed the presence of cleaved PARP product which was preceded by the appearance of p17, the catalytically active fragment of caspase-3. Mitochondrial function assays revealed a MOI dependent decrease in cell viability at 24 h post-infection (pi). No appreciable modifications in Bcl-2, Bcl-X_L and Bax protein levels were observed upon CVB3 infection during 5–24 h observation period. However, a marked decrease in pro-apoptotic Bad abundance was detected without changes in its mRNA levels. In this study we found that the hESCs are highly susceptible to CVB3 infection and display elevated apoptosis rates, thus emerging as suitable human non-transformed in vitro models to study CVB3-induced apoptosis and resulting relevant to understand CVBs pathogenesis.

Keywords Human embryonic stem cells · Coxsackievirus B3 · Apoptosis · Bcl-2 family members

Abbreviations

hESCs	Human embryonic stem cells
CVB3	Coxsackie virus B3
H5	HUES-5 cell line

L. Romorini · M. E. Scassa · G. V. Richardson · C. Blüguermann · M. Questa · D. D. Fernandez Espinosa · G. E. Sevlever · S. G. Miriuka (✉)
Laboratorio de Biología del Desarrollo Celular, LIAN, FLENI, Ruta 9, Km 52,5, Escobar, B1625XAF Buenos Aires, Argentina
e-mail: smiriuka@fleni.org.ar

M. E. Scassa
e-mail: mescassa@fleni.org.ar

G. V. Richardson
e-mail: willyvidelar@hotmail.com

C. Blüguermann
e-mail: carobluguer@gmail.com

M. Questa
e-mail: mariaquesta@gmail.com

D. D. Fernandez Espinosa
e-mail: dfernandez@fleni.org.ar

G. E. Sevlever
e-mail: gsevlever@fleni.org.ar

C. J. de Giusti · R. M. Gómez
Instituto de Biotecnología y Biología Molecular, CCT-La Plata, CONICET-UNLP, Calle 49 y 115, 1900 La Plata, Buenos Aires, Argentina
e-mail: caroj84@hotmail.com

R. M. Gómez
e-mail: rmg@biol.unlp.edu.ar; rmg1426@yahoo.com.ar

H1	WA01 cell line
MOI	Multiplicity of infection
PARP	Poly-ADP-ribose-polymerase
CAR	Coxsackievirus-adenovirus receptor
DAF	Decay accelerating factor
VP1	Viral protein 1
Ac-DEVD*pNA*	Acetyl-Asp-Glu-Val-Asp-7-amino-4 p-nitroanilide
iMEF	Inactivated mouse embryonic fibroblast
KSR	Knockout Serum Replacement
DAPI	4-6-Diamidino-2-phenylindole
XTT	2,3-bis (2-methoxy-4-nitro-5-sulfophenyl)-5 [(phenylamino) carbonyl]-2 H-tetrazolium hydroxide
PMS	*N*-methyl dibenzopyrazine methyl sulfate
BCA	Bicinchoninic acid
Pi	Post-infection
Cpe	Cytopathic effect
TUNEL	Terminal dUTP nick end labeling

Introduction

Human embryonic stem cells (hESCs) are pluripotent cells derived from the inner cell mass of early human embryos that are capable of in vitro differentiation into virtually every cell type found in the adult body. In addition, these cells can self-renew and be cultured indefinitely in vitro. Therefore, hESCs hold great promise as models for human development and disease, as well as for drug discovery and cell-replacement therapies [1, 2].

Coxsackievirus B3 (CVB3), a non-enveloped single positive-polarity RNA *enterovirus* in the *Picornaviridae* family, enters into host cells through binding to the coxsackievirus-adenovirus receptor (CAR) [3]. The virion morphology is characterized by a star-shaped mesa at each fivefold icosahedral symmetry axis, surrounded by a narrow depression ("canyon"), formed by the viral capsid proteins VP1-VP2-VP3, which binds to CAR [4]. Receptor binding induces conformational changes, which facilitate the internalization of viral RNA into host cells [5, 6]. Additionally, decay accelerating factor (DAF) acts as an attachment but not an entry receptor for CVB3 [7, 8].

CVB3 infection is the most frequent cause of human viral myocarditis in neonates, children and young adults [9, 10]. CVB3 can also infect other organs such as pancreas, spleen and brain causing severe pathological complications including pancreatitis, non-septic meningitis and encephalitis [9, 11]. Moreover, newborn babies also are considered to be in danger from CVB infection [12, 13]. Some reports concluded that CBV may be an important causative agent in spontaneous abortions and also in stillbirths, as CVBs were isolated from placental and fetal tissues from spontaneous abortions. IgM antibodies to CVB serotypes 1–5 were detected in 42% of women with miscarriage before the 13th week of gestation [14–17]. Interestingly, Feuer et al. [18] demonstrated that CVB3 preferentially targets proliferating neural stem cells located in the neonatal murine central nervous system.

Apoptosis is a distinct type of programmed cell death, which is defined by cellular phenotypic changes including nuclear chromatin condensation, DNA fragmentation, caspases activation, membrane blebbing and cell shrinkage [19, 20]. Apoptosis is induced via two main routes involving either mitochondria (the intrinsic pathway) or death receptors (the extrinsic pathway). Both pathways converge into a common cell death machinery [21]. In the mitochondrial-mediated pathway, cytochrome *c* plus other pro-apoptotic factors, are released from mitochondria and trigger the activation of caspases (initiator caspase-9 and effector caspases 3, 6 and 7) [22, 23]. Caspases cause cell death by cleaving a number of cellular proteins including nuclear lamins [24], DNA repair enzymes such as poly-ADP-ribose-polymerase (PARP) [25], and cytoskeletal proteins such as actin [26].

Mitochondrial mediated apoptosis is controlled at several intracellular check points. One of these is mainly regulated by different members of the Bcl-2 family, which can play opposite functions on programmed cell death. Bcl-2 is an inhibitor of the mitochondrial apoptotic pathway. This anti-apoptotic protein acts to inhibit cytochrome *c* release thereby blocking caspase activation and the apoptotic process [27]. In addition to Bcl-2, a number of other proteins like Bcl-X_L, Bcl-w and Mcl1, have an anti-apoptotic effect. On the other hand, the members of the pro-apoptotic group include Bax, Bad, Bak, Bid, Bim, among others [28]. Bax and Bak proteins, in particular, upon an apoptotic stimulus, are responsible of the mitochondrial outer membrane permeabilization that allows cytochrome *c* release [29, 30]. In contrast, other pro-apoptotic proteins, like Bad, disrupt the function of anti-apoptotic Bcl-2 family members by kidnapping them on cytoplasm [31, 32].

Apoptosis is one of the hallmarks of viral infection. In several infection models, apoptotic events appear to provide a defense mechanism whereby the infected cell commits suicide prior to the completion of virus life cycle, limiting virus replication [33]. In such circumstances, the apoptotic bodies are eventually recognized and cleared by neighboring phagocytic cells. However, in some other systems, virus-induced apoptosis seems to facilitate viral progeny release from infected cells enhancing viral spread and disease progression [34, 35]. On this sense, it has been demonstrated that a hallmark of CVB3-induced

pathogenesis is apoptosis as previous studies have shown that apoptotic events occur frequently during CVB3 infections under in vitro as well as in vivo conditions [36–39]; hence, the activation of apoptotic pathways during CVB3 infection is of growing interest and many details regarding CVB3 involvement in the apoptosis processes still remain unclear [40].

HeLa cells are the most common human in vitro model used to study CVB3 infection and apoptosis. Activation of the apoptotic machinery has been demonstrated in HeLa cells following CVB3 infection [39, 41, 42]. However, as conclusions made from tumor-derived cells lines are always subject of controversy, new non-cancerous cell based in vitro models are desirable. Host cell status plays an important role in determining CVB3 infection outcome. In this regard, highly proliferative cells, like HeLa, appeared to be more susceptible to productive CVB3 infections [43]. On this sense, it was recently reported that non-transformed highly replicative human embryonic stem cell lines robustly express CAR and DAF receptors and are susceptible to CVB1–5 strains infection. Importantly, IFN-Iβ treatment significantly reduced viral replication, suggesting that type I IFN signalling is also involved in the control of CVB infection in these cells [44]. hESCs emerged then as good candidates to study CVB3-induced cytopathic effects, and because of that we aim to determine the mechanisms of cell death triggered by CVB3 infection in hESCs.

In the present study we found that CVB3 infection decreased cell viability and increased chromatin condensation, DNA fragmentation, caspase-9 cleavage, caspase-3 activation and PARP cleavage in hESC lines WA01 (H1) and HUES-5 (H5). Therefore, CVB3 infection induces apoptosis of hESCs. Moreover, no relevant changes in Bcl-2 family members mRNA and protein expression levels were found, except for Bad protein, which is down-regulated after virus infection. These findings are relevant for understanding the mechanisms of CVB3 cytopathic effects in hESCs.

Materials and methods

Cell lines and culture

The human embryonic stem cell (hESC) line WA01 (H1) was purchased from WiCell Research Institute (WI), and the hESC line HUES-5 (H5) was acquired from Harvard University and the Howard Hughes Medical Institute (MA) at low passages (p15 to p20). The hESC lines were maintained on an inactivated mouse embryonic fibroblast (iMEF) feeder layer in medium comprised of Dulbecco's Modified Eagle's Medium/Ham's F12 (DMEM/F12) supplemented with 10% Knockout Serum Replacement (KSR), 2 mM nonessential amino acids, 2 mM L-glutamine, 100 U/ml penicillin, 50 μg/ml streptomycin, 0.1 mM β-mercaptoethanol and 4 ng/ml of bFGF. All these reagents were obtained from Invitrogen (Carlsbad, CA, USA). hESCs were transferred with 1 mg/ml collagenase IV (Invitrogen, CA, USA) into feeder-free diluted (1/40) Matrigel™ (BD Bioscience, San Jose, CA, USA) coated dishes containing iMEF conditioned medium. For the conditioning medium, 3×10^6 inactivated MEFs were incubated for 24 h with 25 ml of DMEM/F12 medium supplemented with 5% KSR and 2 ng/ml of bFGF (in addition to the other aforementioned supplements) and stored at −20°C. After thawing, fresh aliquots of KSR and bFGF were added to the medium to render a final concentration of 20% and 8 ng/ml, respectively. Before experiments, hESCs grown on Matrigel™ were dissociated into single cells using accutase 1× (Invitrogen, CA, USA) for 20 min, plated onto Matrigel™ coated dishes (with addition of 10 μM Y-27632 ROCK inhibitor) and grown until confluence with conditioned medium.

HeLa cells used for virus propagation and viral titrations were maintained as monolayers in MEM supplemented with 10% (vol/vol) FBS, 2 mM L-glutamine, 25.5 mM sodium bicarbonate and 50 μg of gentamicin/ml.

Virus

CVB3 (Nancy strain) was obtained from the American Tissue Culture Collection (ATCC). The viral stocks were prepared by partially purifying the virus through a 30% sucrose cushion, as previously described [45].

Cell infection

hESCs were infected with a multiplicity of infection (MOI) of 0.01, 0.1, 1 or 10 for 1 h at 37°C. Mock infection was performed by replacing the same volume of virus inoculum with uninfected HeLa cells supernatant. The cells were then washed and maintained in conditioned medium.

Immunostaining and fluorescence microscopy

hESCs were analyzed for in situ immunofluorescence. Briefly, the cells were rinsed with ice-cold PBS and fixed in PBSA (PBS with 0.1% bovine serum albumin) with 4% formaldehyde for 45 min. After two washes cells were permeabilized with 0.1% Triton X-100 in PBSA with 10% normal goat serum for 30 min, washed twice and stained with the corresponding primary antibodies: murine monoclonal antibodies (mAb) anti-SSEA4 (clone 813-70), anti-Tra-1-60 (TRA-1-60), anti-Tra-1-81 (sc-21706), anti-Oct-3/4 (clone C-10), rabbit polyclonal anti-Nanog (clone H-155) and anti-VP1 from Santa Cruz Biotechnology

(Santa Cruz, CA, USA). Fluorescent secondary antibodies fluorescein isothiocyanate (FITC)-conjugated anti-mouse IgG, FITC-conjugated anti-rabbit IgG, Texas Red-X (TR)-conjugated anti-rabbit IgG and TR-conjugated anti-mouse IgG were purchased from Molecular Probes/Invitrogen (Carlsbad, CA, USA) and were used to localize the antigen/primary antibody complexes. The cells were counterstained with 4-6-diamidino-2-phenylindole (DAPI) (Molecular Probes/Invitrogen, Carlsbad, CA, USA) and examined under a Nikon Eclipse TE2000-S inverted microscope equipped with a 20× E-Plan objective and a super high-pressure mercury lamp. The images were acquired with a Nikon DXN1200F digital camera, which was controlled by the EclipseNet software (version 1.20.0 build 61).

Cell viability assay

hESCs were plated onto Matrigel™ coated 96-well tissue culture plates at densities between 1×10^4 and 3×10^4 cells per well and grown until confluence. 24 h post-infection (pi), 50 µg/well of activated 2,3-bis (2-methoxy-4-nitro-5-sulfophenyl)-5 [(phenylamino) carbonyl]-2 H-tetrazolium hydroxide (XTT) (Sigma, St. Louis, MO, USA) in PBS containing 0.3 µg/well of the intermediate electron carrier, *N*-methyl dibenzopyrazine methyl sulfate (PMS) (Sigma, St. Louis, MO, USA) were added (final volume 100 µl) and incubated for 1–2 h at 37°C. Cellular metabolic activity was determined by measuring the absorbance of the samples with a multiplate spectrophotometer (Benchmark, Bio-Rad, Hercules, CA, USA) at a wavelength of 450 nm and subtracting the background absorbance at 690 nm.

TUNEL assay

An in situ cell death detection kit using TdT-mediated fluorescein-conjugated dUTP nick end labeling (TUNEL, In Situ Cell Death Detection Kit Fluorescein, AP; Roche Molecular Biochemicals, Mannheim, Germany) was used to detect apoptotic cells following manufacturer's instructions. The procedure, using a photometric enzyme immunoassay, determines cytoplasmic histone-associated DNA fragments (mono- and oligonucleosomes) after cell death. Fluorescein labels were detected by fluorescence and examined under a Nikon Eclipse TE2000-S inverted microscope equipped with a 20× E-Plan objective and a super high-pressure mercury lamp. The images were acquired with a Nikon DXN1200F digital camera, which was controlled by the EclipseNet software (version 1.20.0 build 61). Densitometric analyses were performed with ImageJ 1.34s software (Wayne Rasband, National Institutes of Health, USA. http://rsb.info.nih.gov/ij/).

Caspase-3 like activity

Caspase-3-like activity was measured by a colorimetric assay. In brief, hESCs were plated in Matrigel™ coated p60 plates, incubated in conditioned medium at 37°C until confluence and then infected with CVB3 as described above. At 1 h pi, cells were lysed in 50 mM Tris–HCl buffer pH 7.4 containing 1 mM EDTA, 10 mM EGTA, 10 µM digitonin, 0.5 mM PMSF, 1.54 µM aprotinin, 14.58 µM pepstatin and 63.86 µM benzamidine, for 30 min at 37°C. Cell lysates were clarified by centrifugation and 150 µl of the resultant supernatant (100–200 µg protein) were incubated with 146 µl of incubation buffer (100 mM HEPES pH 7.5, 20% glycerol, 0.5 mM EDTA and 5 mM dithiothreitol (DTT)) and 4 µl of the substrate acetyl-Asp-Glu-Val-Asp-7-amino-4 *p*-nitroanilide (Ac-DEVD*pNA*) (100 µM) at 37°C for different times (2 and 4 h). Caspase-catalyzed release of the chromophore *pNA* from the substrate was measured at 405 nm with a multiplate spectrophotometer (Benchmark, Bio-Rad, Hercules, CA, USA) and the cleavage activity was expressed as pNA absorbance units/mg protein. Blanks containing either the substrate or the cell lysate alone were subtracted from the A405 nm values of the corresponding test wells. Protein concentration was determined with a BCA Protein Assay Kit (Pierce Thermo Scientific, Rockford, IL, USA) using bovine serum albumin as standard.

RNA isolation, RT-PCR and RT-qPCR

Total RNA was extracted from hESCs with Trizol (Invitrogen, Carlsbad, CA, USA) as recommended by the manufacturer. cDNA was synthesized from 500 ng of total RNA with 15 mM of random hexamers (Invitrogen, Carlsbad, CA, USA) and MMLV reverse transcriptase (Promega, Madison, WI, USA), according to manufacturer's instructions. The cDNA samples were diluted five-fold, and the PCR reaction was conducted at an annealing temperature of 55°C. All of the reactions were within the linear range of amplification. For the qPCR studies, PCR amplification and analysis were performed with ABI PRISM 7500 Sequence Detector System (PE Applied Biosystems, Foster City, CA, USA). The SYBR® Green-ER™ qPCR SuperMix UDG (Invitrogen, Carlsbad, CA, USA) was used for all reactions, following manufacturer instructions. A melting curve analysis was performed immediately after amplification at a linear temperature transition rate of 0.3°C/s from 70 to 89°C with continuous fluorescence acquisition. After qPCR, the amplicon size was confirmed by gel electrophoresis. The primers sequences and sizes of the amplified fragments are shown in Table 1.

Table 1 Primers used for RT-PCR and qPCR experiments and size of fragments

Name	Fragment size (bp)	Prime sequence (5′-3′)	
		Forward	Reverse
Oct-4	126	CTGGGTTGATCC TCGGACCT	CACAGAACTCATACGGCGGG
Nanog	109	AAAGAATCTTCACCTATGCC	GAAGGAAGAGGAGAGACAGT
Gapdh	98	ACAGCCTCAAGATCATCAG	GAGTCCTTCCACGATACC
Bcl-2	240	TATAACTGGAGAGTGCTGAAG	ACTTGATTCTGGTGTTTCCC
Bcl-x_L	284	TGCGTGGAAAGCGTAGACAAG	GTGGGAGGGTAGAGTGGATGG
Bax	195	GACGGCAACTTCAACTGG	GTGAGGAGGCTTGAGGAG
Bad	177	ATGAGTGACGAGTTTGTGGAC	CGGGATGTGGAGCGAAGG

Protein analysis

Total proteins were extracted from hESCs in ice-cold RIPA protein extraction buffer (50 mM Tris–HCl, 150 mM NaCl, 1% triton, 0.25% sodium deoxycholate, 1 mM EDTA pH 7.4) supplemented with protease inhibitors (Protease inhibitor cocktail set I, Calbiochem, San Diego, CA, USA). The lysates were centrifuged at 14,300×*g* and 4°C for 10 min, and the pellet discarded. Cleared lysates were combined with SDS sample buffer (50 mM Tris pH 6.8, 1% SDS, 0.1% bromphenol blue, 10% glycerol, 100 mM DTT). For western blot, samples were boiled for 5 min and electrophoresed for 3 h at 100 V in 15% or 10%, SDS–polyacrylamide gel, transferred to a PVDF membrane (Bio-Rad, Hercules, CA, USA) by electroblotting in transfer buffer containing 20% methanol (vol/vol), 0.19 M glycine, 0.025 M Tris-base (pH 8.3) at 10 V for 45 min (Trans-Blot SD Semi-Dry Electrophoretic Transfer Cell, Bio-Rad, Hercules, CA, USA). Blots were blocked 1 h at room temperature in TBS (20 mM Tris–HCl, pH 7.5, 500 mM NaCl) containing low-fat powdered milk (5%) and Tween 20 (0.1%). Incubations with primary antibodies were performed at 4°C for 12 h in blocking buffer (3% skim milk, 0.1% Tween, in Tris-buffered saline). The membranes were then incubated with the corresponding counter-antibody and the proteins evidenced by enhanced chemiluminescence detection (SuperSignal West Femto System, Thermo Scientific, Rockford, IL, USA). The following primary antibodies were used: α-Bcl-$X_{L/S}$ (sc-634); α-Bax (sc-493); α-Bcl-2 (sc-7382); α-Bad (sc-943); α-PARP (sc-8007) and α-Actin (sc-1616) (Santa Cruz Biotechnology, Santa Cruz, CA, USA), α-active Caspase-3 (ab13847) (Abcam Inc., Cambridge, MA, USA) and α-caspase-9 (cat. 9502) (Cell Signaling Technology, Beverly, MA, USA). As secondary antibodies the following were used: a horseradish peroxidase-conjugated α-rabbit IgG; α-mouse IgG or α-goat IgG. Densitometric analysis of protein levels were performed with ImageJ 1.34s software (Wayne Rasband, National Institutes of Health, USA. http://rsb.info.nih.gov/ij/).

Statistical analysis

All results are expressed as mean ± SEM. For XTT experiments one-way ANOVAs followed by Tukey's multiple comparisons tests were used to detect significant differences among treatments ($P < 0.05$). The student's paired *t* test was used to determine significant differences between means for DAPI and TUNEL studies ($P < 0.05$).

Results

Analysis of stem cell markers expression and susceptibility to CVB infection of human embryonic stem cells grown as monolayer

We first validated the pluripotent nature of HUES-5 (H5) and WA01 (H1) hESC lines grown as monolayer until confluence on Matrigel™ coated culture dishes. Experiments were conducted on feeder-free conditions to avoid contamination with MEFs. hESCs exhibited robust expression of stem cells associated markers, such as nuclear located transcription factors Oct-4 and Nanog and surface markers SSEA-4, TRA1-60 and TRA1-81 (Fig. 1a). The tested cell lines also expressed transcripts associated with pluripotency such as *oct-4* and *nanog* (Fig. 1b). These results show maintenance of pluripotent characteristics under the experimental conditions used.

Then, H5 and H1 cells were infected with CVB3 and the intracellular presence of viral structural protein VP-1 was assessed by immunostaining at 16 h pi. A high proportion of cells resulted immunoreactive for VP-1 thus confirming hESCs susceptibility to CVB3 virus infection (Fig. 1c).

CVB3 infection induces apoptosis of human embryonic stem cells

We next evaluated how CVB3 infection affects hESCs viability. As shown in Fig. 2a, after 24 h of CVB3 infection the number of viable cells felt down to 21 ± 13.8% for

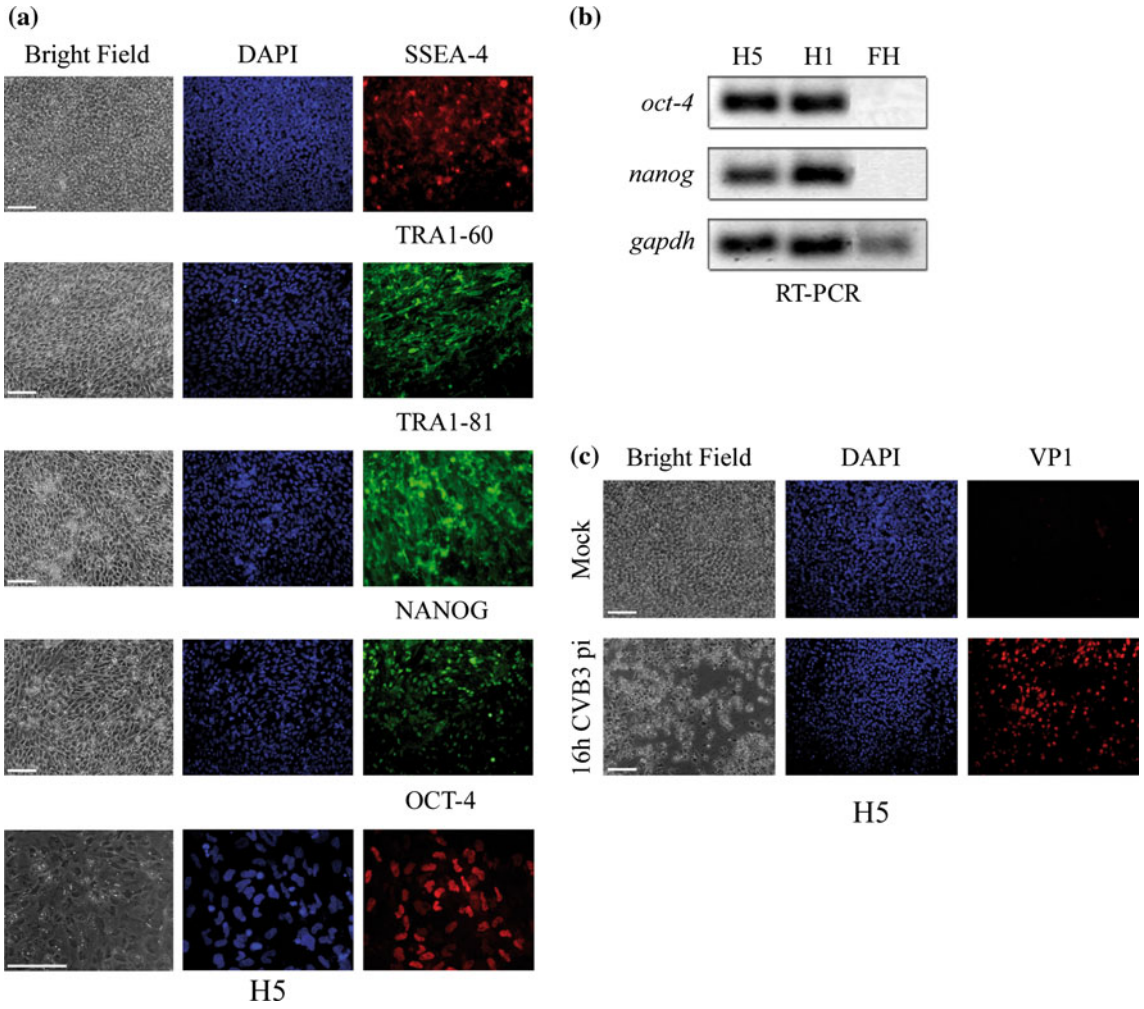

Fig. 1 Expression of stem cell markers and intracellular presence of viral VP1 protein. **a** Immunofluorescence staining of confluent HUES-5 (H5) hESCs grown on Matrigel™ coated plates and fixed and stained with primary antibodies recognizing stem cell markers. Figure shows representative images of hESC stained with SSEA-4, TRA-1-60, TRA-1-81, Nanog and Oct-4. The nuclei were counterstained with DAPI. The scale bars represent 100 and 200 μm. **b** RT-PCR analysis of stem cell-like transcripts *nanog* and *oct-4* was performed on feeder-free confluent undifferentiated H5 and WA01 (H1) hESCs. *gapdh* was used as loading control. **c** Figure shows representative images of feeder-free confluent undifferentiated H5 cells at 16 h CVB3 pi and immunostained for VP1. The nuclei were counterstained with DAPI. Mock: uninfected control cells. The *scale bars* represent 100 μm. *Abbreviations*: *SSEA-4* stage-specific embryonic antigen, *TRA-1-60* tumor rejection antigen 1-60, *TRA-1-81* tumor rejection antigen 1-81, *Oct-4* octamer 4, *VP1* viral protein 1, *CVB3* Coxsackievirus subgroup B, serotype 3, *pi* post-infection

H5 and 23 ± 6.9% for H1. As expected, an increase in cell viability was observed when tenfold serial dilutions of CVB3 were used.

In CVB3-infected hESCs, a cytopathic effect (cpe) characterized by ballooning and cell detachment was observed as soon as 4 h pi (Fig. 2b, upper panels). This cpe is compatible with programmed cell death.

Chromatin condensation paralleled by DNA fragmentation are two of the most important criteria which are used to indentify apoptotic cells, therefore we next measured these processes by DAPI staining of nuclear DNA and TUNEL technique, respectively. CVB3 infection increased the percentage of hESCs DAPI positive apoptotic nuclei as soon as 4 h pi (8.8 ± 2.9% mock, 24.6 ± 1.1% 4 h CVB3 pi, 32.8 ± 3.4% 8 h CVB3 pi for H5 cells; 27.5 ± 6.6% mock, 42.5 ± 4.9% 4 h CVB3 pi, 55.6 ± 5.5% 8 h CVB3 pi for H1 cells) (Fig. 2b, lower panels and graph). In what it concerns to DNA fragmentation, a significant increase in TUNEL-positive cells was found in H5 and H1 hESCs infected with CVB3. Remarkably, TUNEL signals generated at 8 h pi were as high as DNAse I treated cells (3.2 ± 1.1 and 3.4 ± 0.7 fold induction vs. mock for 8 h CVB3 pi H5 and H1 cells, respectively. 4 ± 0.9 fold induction vs. mock for DNAse I treated cells) (Fig. 3a).

Activation of initiator and effector caspases is other relevant criteria to determinate apoptosis induction. Upon CVB3 infection, initiator pro-caspase-9 (47 kDa) was processed into active fragments (37/35 and 17 kDa). A decrease

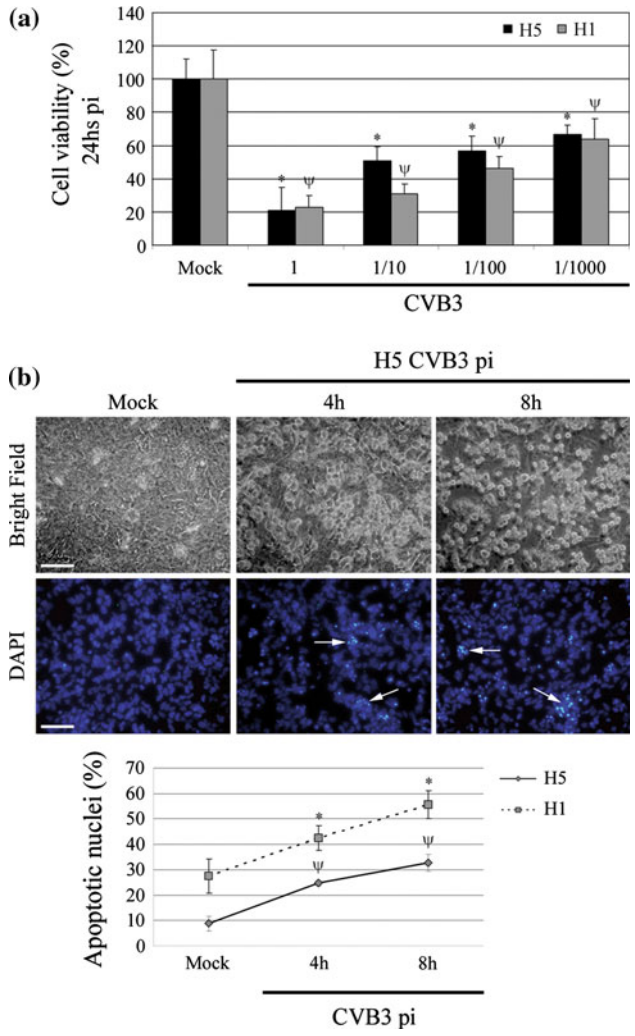

Fig. 2 Cell viability and chromatin condensation changes induced by CVB3 infection in hESCs. **a** Cell viability was assessed by XTT colorimetric assay performed at 24 h H5 and H1 CVB3 pi and is expressed as percentage of the internal control (Mock: mock-infected cells). tenfold serial dilutions of CVB3 were used (MOI between 10 and 0.01). *Bars* indicate Mean ± SE of four replicates from three independent experiments ($n = 12$). * = $P < 0.05$; $\psi = P < 0.05$. **b** Chromatin condensation was analyzed by DAPI staining of feeder-free confluent H5 and H1 hESCs at 4 and 8 h CVB3 pi (MOI = 1). Figure shows representative images and *arrows* indicate apoptotic nuclei. Means ± SE from three independent experiments are graphed for % of apoptotic nuclei. * = $P < 0.05$; $\psi = P < 0.05$

in pro-caspase-9 and an increase in active fragments protein levels were detected (pro-caspase-9 = 0.99 ± 0.04, 0.91 ± 0.04, 0.81 ± 0.17, 0.53 ± 0.08; 17 kDa cleaved caspase-9 = 3.73 ± 1.81, 1.51 ± 0.33, 1.90 ± 0.18, 2.12 ± 0.5 fold induction for 5, 8, 16 and 24 h CVB3 pi, respectively) (Fig. 3b, upper panels and graph). Cleaved caspase-9 could further process other caspase members, including caspase-3, to initiate a caspase cascade, which leads to apoptosis. Western blot detection of cleaved caspase-3 (appearance of caspase-3 p17) revealed a time-dependent activation of caspase-3, concomitant with caspase-9 activation, mediated by CVB3 infection (2.5 ± 0.05, 2.4 ± 0.3, 3.85 ± 1.1, 12.3 ± 0.7 fold induction for 5, 8, 16 and 24 h CVB3 pi, respectively) (Fig. 3b, middle upper panel and graph). In parallel, caspase-3 activity was assessed by two different experimental approaches: PARP cleavage by western blot and *p*-nitroanilide release from acetyl-DEVD-*p*-nitroanilide by spectrophotometric detection. Time course studies revealed the presence of cleaved PARP which was preceded by the appearance of catalytically active p17. This chronology is compatible with the involvement of caspase-3 in PARP proteolysis (Fig. 3b middle lower panel and graph). By other hand, caspase-3 enzyme activity is detected as soon as 1 h CVB3 pi (1.9 and 1.7 fold induction vs. mock for H5 and H1, respectively) (Fig. 3c).

Taken together, these results indicate that CVB3 infection induces apoptosis of hESCs and that, based on caspase-9 cleavage, the mitochondrial-mediated apoptosis pathway may participate in this induction.

Bcl-2 family members expression levels after CVB3 infection

Western blot assays were performed in order to analyze protein expression levels of Bcl-2 family members in hESCs after CVB3 infection. Results shown in Fig. 4a indicate that neither anti-apoptotic proteins Bcl-2 and Bcl-X_L nor pro-apoptotic protein Bax changed up to 24 h CVB3 pi (first, second and third panels, respectively and graph). On the contrary, pro-apoptotic Bad protein levels decreased upon CVB3 infection (0.41 ± 0.21 and 0.28 ± 0.17 fold induction vs. mock for 16 and 24 h CVB3 pi, respectively) (Fig. 4a fourth panel and graph). mRNA level analysis by RTqPCR revealed that *bad* expression in H5 and H1 hESCs is not affected by CVB3 infection (Fig. 4b). Bad protein down-regulation may be then due to changes in protein stabilization and not to mRNA levels. The rest of the Bcl-2 family members mRNA levels studied only showed slight down-regulations for *bcl-x*$_L$ and *bax*. However these variations were not reflected at the protein level (Fig. 4a, b).

Discussion

One of the potential mechanisms by which CVB3-infected cells die is apoptosis [46]. Understanding how CVB3 are capable of modulating host apoptotic balance is of major interest for the development of new therapeutic strategies against CVB3-related diseases and therefore for the control of the viral spread in different tissues.

CVB3 is a frequent cause of severe diseases and pathological complications [9, 11]. Moreover, it has been

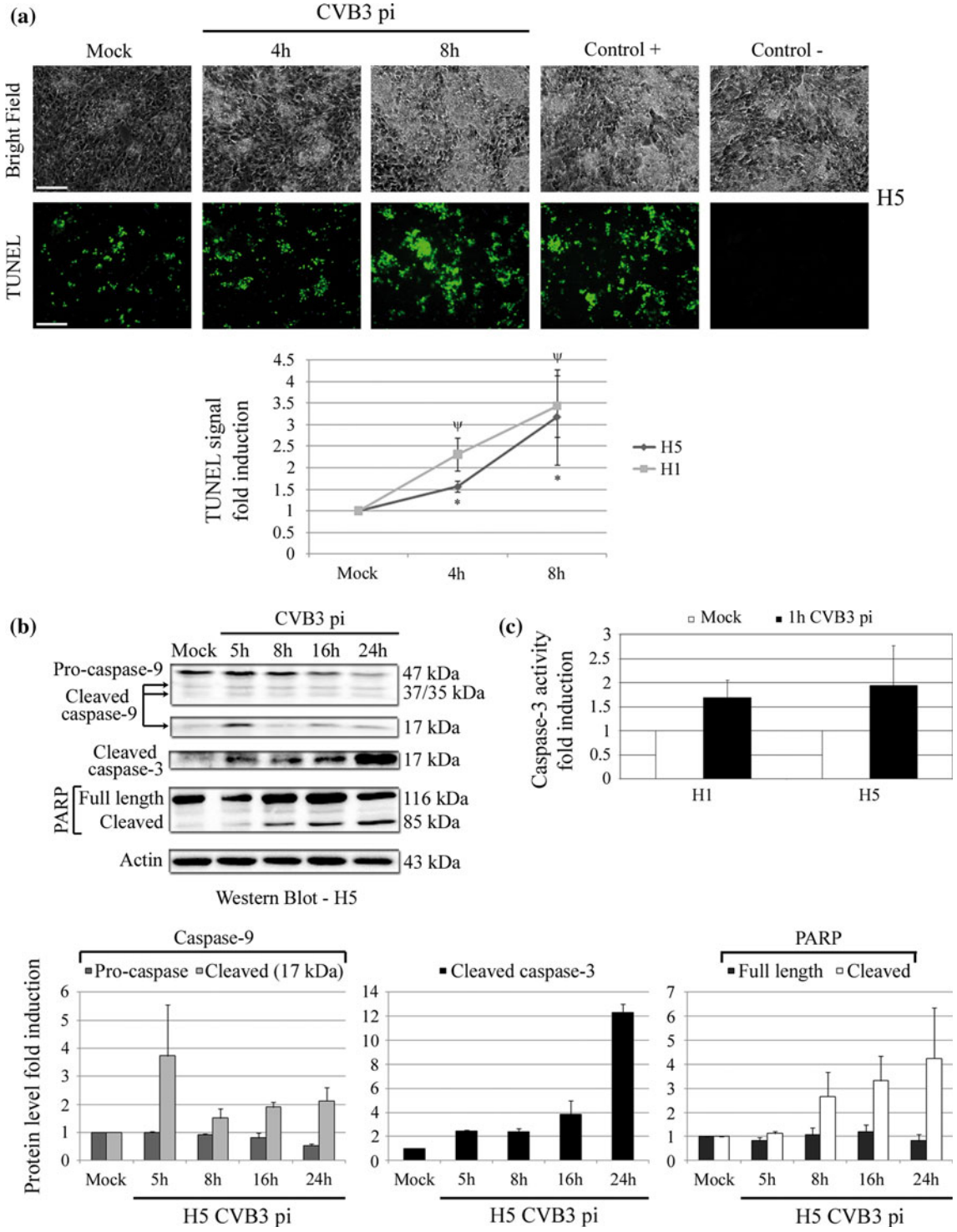

demonstrated that newborn mice are more susceptible than adult mice to group B Coxsackie viruses. The most likely mechanism involved is the diminution in the abundance of cellular receptors with age, since viral cellular receptors (CAR and DAF) are major determinants of CVB3 pathogenesis [47]. In this sense, it was reported that hESCs robustly express CVB receptors CAR and DAF and are susceptible to CVB3 infection. In particular, CAR transcripts were always more abundant in hESCs than in differentiated counterparts obtained using embryoid body

◀ **Fig. 3** DNA fragmentation and caspase-3 activity induced by CVB3 infection in hESCs. **a** DNA fragmentation was assessed by TUNEL assay performed in H5 and H1 at 4 and 8 h CVB3 pi (MOI = 1) and is expressed as TUNEL signal fold induction of the internal control (Mock: mock-infected cells). Positive control: mock-infected cells treated with DNAse I. Negative control: mock-infected cells in label solution only (without terminal transferase). Representative images are shown and the Means ± SE from three independent experiments are graphed. The *scale bars* represent 100 µm. * = $P < 0.05$; $\psi = P < 0.05$. **b** Confluent feeder-free H5 cells were infected with CVB3 (MOI = 0.1) and cell lysates prepared and analyzed by western blot at 5, 8, 16 and 24 h pi. Membranes were probed with antibodies against Caspase-9 (*upper panel*), active cleaved Caspase-3 (*middle upper panel*), PARP (*middle lower panel*) and Actin (*lower panel*) proteins. Representative blots from three independent experiments are shown. Pro-caspase-9, cleaved caspase-9 (17 kDa), cleaved caspase-3 and PARP (Full length and cleaved) protein expression are expressed as fold induction relative to controls (Mock: mock-infected cells). Means ± SE from three independent experiments are shown (B, column graph). **c** Caspase-3 activity was determined 1 h post CVB3-infection in H5 and H1 (MOI = 1) by measuring the proteolysis of Ac-DEVD*pNA* during 2–4 h. Specific activity was calculated as A405/mg protein under the standard incubation conditions and expressed as fold induction against the internal control (Mock: mock-infected cells). Means ± SE from three independent experiments are shown

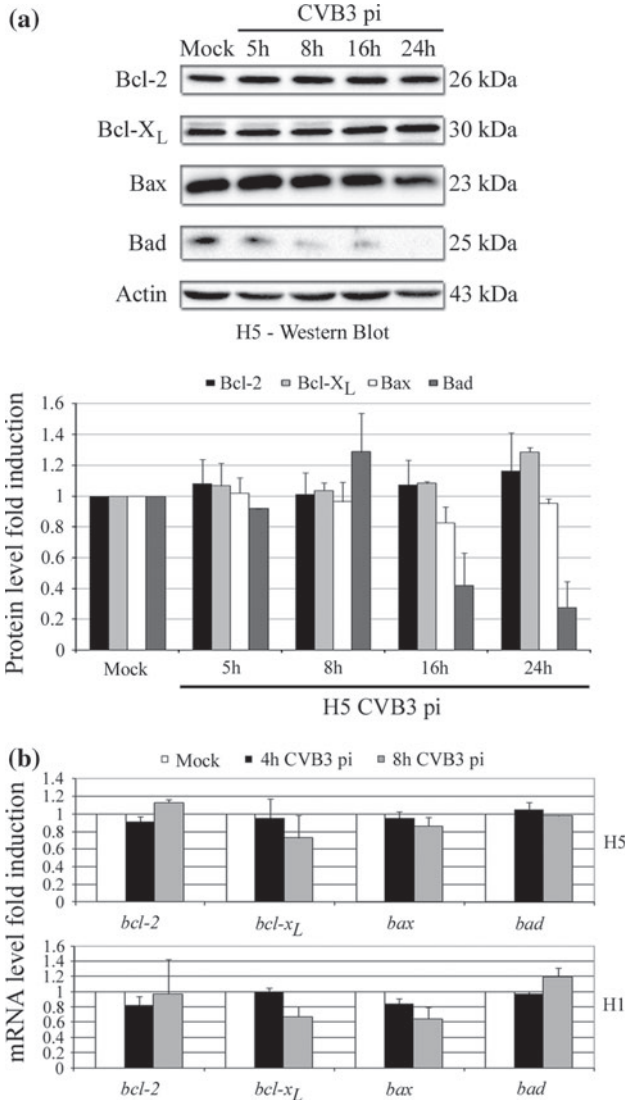

Fig. 4 Bcl-2 family members expression levels changes after CVB3 infection of hESCs. **a** Confluent feeder-free H5 cells were infected with CVB3 (MOI = 0.1) and cell lysates prepared and analyzed by western blot at 5, 8, 16 and 24 h pi. Membranes were probed with antibodies against Bcl-2 (*upper panel*), Bcl-X_L (*middle upper panel*), Bax (*middle middle panel*), Bad (*middle lower panel*) and Actin (*lower panel*) proteins. Representative blots from three independent experiments are shown. Bcl-2, Bcl-X_L, Bax and Bad protein levels are expressed as fold induction relative to controls (Mock: mock-infected cells). Means ± SE from three independent experiments are shown (A, column graph). **b** mRNA expression levels were analyzed by qPCR in H5 and H1 at 4 and 8 h after CVB3 infection (MOI = 0.1) with primers that amplified *bcl-2, bcl-x$_L$, bax* and *bad. Actin* expression was used as normalizer. Graph shows mRNA fold induction relative to the controls (Mock: mock-infected cells). The Means ± SE from three independent experiments are shown

based hESCs-differentiation protocol [44]. Taken together, all these observations make the study of the mechanisms of cell death triggered by CVB3 virus infection in hESCs of growing interest.

In the present study, we assessed for the first time the impact of CVB3 infection on hESCs apoptosis. We found, by measuring chromatin condensation (DAPI staining) and DNA fragmentation (TUNEL assay), that apoptosis induction occurs as soon as 4 h CVB3 pi in H5 and H1 hESC lines. Moreover, at 8 h pi 32.8 and 55.6% of H5 and H1 nuclei, respectively, exhibit apoptotic features. It is important to mention that H1 cell line showed higher apoptotic basal levels than H5 cell line (8.8 vs. 27.5% of apoptotic nuclei, respectively). Importantly, these differences between hESCs lines have been already reported and it is known that in some hESCs lines >30% of the cells undergo spontaneous apoptosis under routine culture conditions [48]. These findings suggest that CVB3 infection may induce faster and higher apoptosis rates in hESCs than in HeLa cells [38].

The mitochondria-mediated pathway is commonly believed to be associated with apoptosis induced by CVB3, thus caspase activation [39, 49] and mitochondrial release of cytochrome *c* [41] may be important early events in CVB3 infection. Further studies showed that in addition to caspase-3 activation, multiple members of the caspase family (caspase-2, 6, 7, 8 and 9) were activated or degraded during CVB3 infection in HeLa cells and in murine atrial cardiomyocytes [41]. Moreover, Bcl-2 or Bcl-X_L overexpression markedly reduced cytochrome *c* release, depressed caspase activation, delayed the loss of host cell viability and decreased progeny virus release following infection [41]. Our results demonstrated that initiator caspase-9 and effector caspase-3 are cleaved in hESCs upon CVB3 infection and that the cleaved caspase-3 is proteolytically active (confirmed by caspase activation assays and

PARP cleavage). Thus, the mitochondrial-mediated apoptosis pathway may participate in CVB3 apoptosis induction also in hESCs. Again, hESCs may be more vulnerable than HeLa cells to CVB3 mediated apoptosis, as caspase-3 and PARP cleavage were detected at 5 and 8 h pi, respectively, in hESCs (MOI = 1) and only at 8 and 9 h pi in HeLa cells (MOI = 5) [39]. Beside, an increase in caspase-3 enzymatic activity was detected in hESCs as soon as 1 h pi.

Little is known about how CVB3 infection affects Bcl-2 family members expression levels. It was shown that myocardial mRNA levels of Bax and Bcl-X_L were significantly increased from day 3 onwards in CVB3 infected BALB/c mice [50]. Moreover, it was found that also Bax and Bcl-2 proteins were up-regulated on myocardium of C3H/HeJ mice infected with CVB3 [51, 52]. However, no changes have been seen in our hESCs in vitro model in Bcl-2, Bcl-X_L and Bax protein and mRNA levels upon hESCs CVB3 infection. In contrast, Bad protein is down-regulated under these experimental conditions as soon as 5 h CVB3 pi. *Bad* mRNA expression is not affected in hESCs by CVB3, so Bad protein down-regulation may be due to changes in protein stabilization and not to mRNA levels. According to published reports, Bad protein stability may be affected by ubiquitylation and proteasomal degradation [53] or by a 26S proteasome independent degradation system based on non caspase cytosolic proteases [54, 55]. The mechanism involved in Bad down-regulation in CVB3-infected hESCs still needs to be addressed. However, it is possible that CVB3 viral proteases 2A and 3C could participate in Bad degradation, as it is known that caspase-3, PARP and other substrates are cleaved by ectopic expression of these proteases in HeLa cells [24, 25].

Conclusion

Human embryonic stem cells present high susceptibility to CVB3 infection and apoptosis induction and emerged then as a good human non-tumoral in vitro cell model to study CVB3-induced apoptosis. Moreover, detailed studies of the mechanisms and signaling pathways involved in CVBs apoptosis regulation in hESCs will provide information that may result clinically relevant to understand CVBs pathogenesis. It would allow, among others, to study if susceptibility changes upon differentiation of hESCs into specific lineages by means of defined protocols.

Acknowledgments This work was supported by grants from Agencia Nacional de Promoción Científica y Tecnológica (ANPCyT) PID2007-00112, PICT 07-00642 and PICT 07-00028. The authors would like to thank Marcela Cañari for her skillful assistance.

Conflict of interest The authors declare that they have no conflict of interest.

References

1. Thomson JA, Itskovitz-Eldor J, Shapiro SS et al (1998) Embryonic stem cell lines derived from human blastocysts. Science 282:1145–1147
2. Klimanskaya I, Rosenthal N, Lanza R (2008) Derive and conquer: sourcing and differentiating stem cells for therapeutic applications. Nat Rev Drug Discov 7:131–142
3. Bergelson JM, Modlin JF, Wieland-Alter W, Cunningham JA, Crowell RL, Finberg RW (1997) Clinical coxsackievirus B isolates differ from laboratory strains in their interaction with two cell surface receptors. J Infect Dis 175:697–700
4. Muckelbauer JK, Kremer M, Minor I et al (1995) The structure of coxsackievirus B3 at 3.5 Å resolution. Structure 3:653–667
5. He Y, Chipman PR, Howitt J et al (2001) Interaction of coxsackievirus B3 with the full length coxsackievirus-adenovirus receptor. Nat Struct Biol 8:874–878
6. Rossmann MG (1989) The canyon hypothesis. Hiding the host cell receptor attachment site on a viral surface from immune surveillance. J Biol Chem 264:14587–14590
7. Bergelson JM, Cunningham JA, Droguett G et al (1997) Isolation of a common receptor for Coxsackie B viruses and adenoviruses 2 and 5. Science 275:1320–1323
8. Shafren DR, Williams DT, Barry RD (1997) A decay-accelerating factor-binding strain of coxsackievirus B3 requires the coxsackievirus-adenovirus receptor protein to mediate lytic infection of rhabdomyosarcoma cells. J Virol 71:9844–9848
9. Woodruff JF (1980) Viral myocarditis. A review. Am J Pathol 101:425–484
10. Wessely R, Henke A, Zell R, Kandolf R, Knowlton KU (1998) Low-level expression of a mutant coxsackieviral cDNA induces a myocytopathic effect in culture: an approach to the study of enteroviral persistence in cardiac myocytes. Circulation 98:450–457
11. Whitton JL, Cornell CT, Feuer R (2005) Host and virus determinants of picornavirus pathogenesis and tropism. Nat Rev Microbiol 3:765–776
12. Iwasaki T, Monma N, Satodate R, Kawana R, Kurata T (1985) An immunofluorescent study of generalized Coxsackie virus B3 infection in a newborn infant. Acta Pathol Jpn 35:741–748
13. Pavesi G, Gemignani F, Macaluso GM et al (1992) Acute sensory and autonomic neuropathy: possible association with coxsackie B virus infection. J Neurol Neurosurg Psychiatry 55:613–615
14. Basso NG, Fonseca ME, Garcia AG, Zuardi JA, Silva MR, Outani H (1990) Enterovirus isolation from foetal and placental tissues. Acta Virol 34:49–57
15. Frisk G, Diderholm H (1992) Increased frequency of coxsackie B virus IgM in women with spontaneous abortion. J Infect 24:141–145
16. Axelsson C, Bondestam K, Frisk G, Bergstrom S, Diderholm H (1993) Coxsackie B virus infections in women with miscarriage. J Med Virol 39:282–285
17. Nuovo GJ, Cooper LD, Bartholomew D (2005) Histologic, infectious, and molecular correlates of idiopathic spontaneous abortion and perinatal mortality. Diagn Mol Pathol 14:152–158
18. Feuer R, Pagarigan RR, Harkins S, Liu F, Hunziker IP, Whitton JL (2005) Coxsackievirus targets proliferating neuronal progenitor cells in the neonatal CNS. J Neurosci 25:2434–2444
19. Kerr JF, Wyllie AH, Currie AR (1972) Apoptosis: a basic biological phenomenon with wide-ranging implications in tissue kinetics. Br J Cancer 26:239–257
20. Cory S (1995) Regulation of lymphocyte survival by the bcl-2 gene family. Annu Rev Immunol 13:513–543
21. Leist M, Jaattela M (2001) Four deaths and a funeral: from caspases to alternative mechanisms. Nat Rev Mol Cell Biol 2:589–598

22. Li H, Zhu H, Xu CJ, Yuan J (1998) Cleavage of BID by caspase 8 mediates the mitochondrial damage in the Fas pathway of apoptosis. Cell 94:491–501
23. Green DR, Reed JC (1998) Mitochondria and apoptosis. Science 281:1309–1312
24. Lazebnik YA, Takahashi A, Moir RD et al (1995) Studies of the lamin proteinase reveal multiple parallel biochemical pathways during apoptotic execution. Proc Natl Acad Sci USA 92: 9042–9046
25. Lazebnik YA, Kaufmann SH, Desnoyers S, Poirier GG, Earnshaw WC (1994) Cleavage of poly(ADP-ribose) polymerase by a proteinase with properties like ICE. Nature 371:346–347
26. Mashima T, Naito M, Fujita N, Noguchi K, Tsuruo T (1995) Identification of actin as a substrate of ICE and an ICE-like protease and involvement of an ICE-like protease but not ICE in VP-16-induced U937 apoptosis. Biochem Biophys Res Commun 217:1185–1192
27. Kluck RM, Bossy-Wetzel E, Green DR, Newmeyer DD (1997) The release of cytochrome *c* from mitochondria: a primary site for Bcl-2 regulation of apoptosis. Science 275:1132–1136
28. Cory S, Adams JM (2002) The Bcl2 family: regulators of the cellular life-or-death switch. Nat Rev Cancer 2:647–656
29. Green DR, Kroemer G (2004) The pathophysiology of mitochondrial cell death. Science 305:626–629
30. Korsmeyer SJ, Wei MC, Saito M, Weiler S, Oh KJ, Schlesinger PH (2000) Pro-apoptotic cascade activates BID, which oligomerizes BAK or BAX into pores that result in the release of cytochrome *c*. Cell Death Differ 7:1166–1173
31. Letai A, Bassik MC, Walensky LD, Sorcinelli MD, Weiler S, Korsmeyer SJ (2002) Distinct BH3 domains either sensitize or activate mitochondrial apoptosis, serving as prototype cancer therapeutics. Cancer Cell 2:183–192
32. Abastado JP (1996) Apoptosis: function and regulation of cell death. Res Immunol 147:443–456
33. Eick D, Hermeking H (1996) Viruses as pacemakers in the evolution of defence mechanisms against cancer. Trends Genet 12:4–6
34. Bouzar AB, Villet S, Morin T et al (2004) Simian immunodeficiency virus Vpr/Vpx proteins kill bystander noninfected CD4+ T-lymphocytes by induction of apoptosis. Virology 326:47–56
35. Petrovas C, Mueller YM, Katsikis PD (2004) HIV-specific CD8+ T cells: serial killers condemned to die? Curr HIV Res 2:153–162
36. Feuer R, Mena I, Pagarigan RR, Harkins S, Hassett DE, Whitton JL (2003) Coxsackievirus B3 and the neonatal CNS: the roles of stem cells, developing neurons, and apoptosis in infection, viral dissemination, and disease. Am J Pathol 163:1379–1393
37. Saraste A, Arola A, Vuorinen T et al (2003) Cardiomyocyte apoptosis in experimental coxsackievirus B3 myocarditis. Cardiovasc Pathol 12:255–262
38. Yuan JP, Zhao W, Wang HT et al (2003) Coxsackievirus B3-induced apoptosis and caspase-3. Cell Res 13:203–209
39. Carthy CM, Granville DJ, Watson KA et al (1998) Caspase activation and specific cleavage of substrates after coxsackievirus B3-induced cytopathic effect in HeLa cells. J Virol 72:7669–7675
40. Cunningham KA, Chapman NM, Carson SD (2003) Caspase-3 activation and ERK phosphorylation during CVB3 infection of cells: influence of the coxsackievirus and adenovirus receptor and engineered variants. Virus Res 92:179–186
41. Carthy CM, Yanagawa B, Luo H et al (2003) Bcl-2 and Bcl-xL overexpression inhibits cytochrome *c* release, activation of multiple caspases, and virus release following coxsackievirus B3 infection. Virology 313:147–157
42. Luo H, Yanagawa B, Zhang J et al (2002) Coxsackievirus B3 replication is reduced by inhibition of the extracellular signal-regulated kinase (ERK) signaling pathway. J Virol 76:3365–3373
43. Tabor-Godwin JM, Ruller CM, Bagalso N et al (2010) A novel population of myeloid cells responding to coxsackievirus infection assists in the dissemination of virus within the neonatal CNS. J Neurosci 30:8676–8691
44. Scassa ME, de Giusti CJ, Questa M et al (2011) Human embryonic stem cells and derived contractile embryoid bodies are susceptible to Coxsakievirus B infection and respond to interferon I beta treatment. Stem Cell Res 6:13–22
45. Rinehart JE, Gomez RM, Roos RP (1997) Molecular determinants for virulence in coxsackievirus B1 infection. J Virol 71:3986–3991
46. Buenz EJ, Howe CL (2006) Picornaviruses and cell death. Trends Microbiol 14:28–36
47. Xu R, Crowell RL (1996) Expression and distribution of the receptors for coxsackievirus B3 during fetal development of the Balb/c mouse and of their brain cells in culture. Virus Res 46: 157–170
48. Dravid G, Ye Z, Hammond H et al (2005) Defining the role of Wnt/beta-catenin signaling in the survival, proliferation, and self-renewal of human embryonic stem cells. Stem Cells 23:1489–1501
49. Martin U, Jarasch N, Nestler M et al (2007) Antiviral effects of pan-caspase inhibitors on the replication of coxsackievirus B3. Apoptosis 12:525–533
50. Kyto V, Lapatto R, Lakkisto P et al (2004) Glutathione depletion and cardiomyocyte apoptosis in viral myocarditis. Eur J Clin Invest 34:167–175
51. Joo CH, Hong HN, Kim EO et al (2003) Coxsackievirus B3 induces apoptosis in the early phase of murine myocarditis: a comparative analysis of cardiovirulent and noncardiovirulent strains. Intervirology 46:135–140
52. Colston JT, Chandrasekar B, Freeman GL (1998) Expression of apoptosis-related proteins in experimental coxsackievirus myocarditis. Cardiovasc Res 38:158–168
53. Fueller J, Becker M, Sienerth AR, Fischer A, Hotz C, Galmiche A (2008) C-RAF activation promotes BAD poly-ubiquitylation and turn-over by the proteasome. Biochem Biophys Res Commun 370:552–556
54. Romorini L, Coso OA, Pecci A (2009) Bcl-XL mediates epidermal growth factor dependent cell survival in HC11 mammary epithelial cells. Biochim Biophys Acta 1793:496–505
55. Roberts ML, Virdee K, Sampson CP, Gordon I, Parone P, Tolkovsky AM (2000) The combination of bcl-2 expression and NGF-deprivation facilitates the selective destruction of BAD protein in living sympathetic neurons. Mol Cell Neurosci 16:97–110